

DOI:10.1002/ejic.201301288

# One-Pot Solvothermal Coating of Carbon Spheres with ZnS Nanocrystallites and Their Use in the Photodegradation of Dyes

Kanchan M. Samant,<sup>[a]</sup> Jagruti S. Suroshe,<sup>[a]</sup> and Shivram S. Garje\*<sup>[a]</sup>

**Keywords:** Carbon / Composite materials / Nanoparticles / Thin layers / Chemical vapor deposition / Solvothermal synthesis

In the present investigation, an easy approach for the synthesis of nanostructures composed of carbon spheres (CSs) and ZnS was demonstrated. CSs were prepared by aerosol-assisted chemical vapor deposition of toluene at 1050 °C and were characterized by different techniques, including X-ray diffraction, Raman spectroscopy, scanning electron microscopy, transmission electron microscopy, and thermogravimetric analysis. Further, their composite with ZnS nanoparticles (NPs) was synthesized by using solvothermal decompo-

sition of a single-source precursor in the presence of ethylene glycol. The competence of the resultant composite material was tested in the photodegradation of eriochrome black-T and methylene blue, and the results were compared with those obtained for the bare ZnS NPs. The substantial increase in the photodegradation efficiency of the composite is attributed to the large surface area provided by the CSs to the ZnS NPs for dye reduction.

## Introduction

Carbon is a versatile element that exhibits various forms of structures including carbon nanotubes (CNTs), carbon fibers, graphene, carbon spheres (CSs), and fullerenes. Owing to the unusual chemical, optical, electrical, and magnetic properties of these materials, they find applications in many areas such as catalysis, emission devices, electrochemistry, and gas storage. Among these, CSs are considered to be promising candidates as catalyst supports,<sup>[1]</sup> biomaterials,<sup>[2]</sup> adsorbents,<sup>[3]</sup> and anodes in secondary lithium-ion batteries.<sup>[4]</sup> They possess structural uniformity, high thermal stability, large packing density, high chemical inertness, tunable surface properties, and excellent conductivity.<sup>[5]</sup> Various methods have been reported for the synthesis of CSs. Among the synthetic routes, the sacrificial template method is widely used, as it helps to tune the pore size as well as the surface morphology of the CSs. Silica spheres and aluminosilicate spheres are used as templates along with a carbon precursor that gets carbonized in an inert gas to produce hollow CSs.<sup>[6–9]</sup> Sun et al. developed the hydrothermal synthesis of CSs by using sodium dodecyl sulfate (SDS) and glucose as the starting materials.<sup>[10]</sup> Xia et al.

reported a very simple method to prepare well-ordered hollow spheres of mesoporous N-doped carbon by using acetonitrile as a source of carbon.<sup>[11]</sup> Other methods involve chlorination of ferrocene at high temperature, self-assembly of CNTs, and surfactant-assisted chemical vapor deposition (CVD).<sup>[12–17]</sup>

Recently, the inclination towards synthesizing hybrid nanomaterials by surface modification to produce tailored nanostructure materials has effectively increased.<sup>[18–20]</sup> Tremendous work comprising the immobilization of nanoparticles (NPs) of either metal or semiconductor<sup>[21–24]</sup> on CSs is in progress because of the prospective use of these materials in drug delivery, catalysis, energy storage, and separation technologies. Additionally, such hybrid structures successfully modify the properties of the CSs such as crystallinity, electrical conductivity, adsorption properties, and chemical reactivity.<sup>[5,24–26]</sup>

Given that ZnS NPs are wide band gap semiconductors with a band gap energy of 3.7 eV, they find applications in many fields such as optical coatings, solid-state solar cell windows, electrooptic modulators, photoconductors, field-effect transistors, sensors, transducers, and photocatalysis.<sup>[27,28]</sup> Similar to other wide band gap semiconductors, the appreciable role of ZnS NPs in the degradation of dyes and other organic pollutants<sup>[29]</sup> fascinated us to choose it as a coating material on the surface of CSs. As photocatalytic processes are highly susceptible to surface structures and properties, it is quite interesting to study the role of CSs associated with ZnS NPs in photocatalysis. Though there

[a] Department of Chemistry, University of Mumbai, Vidyanagari, Santacruz (East), Mumbai 400098, India  
E-mail: ssgarje@yahoo.com  
ssgarje@chem.mu.ac.in

<http://www.mu.ac.in/science/chemistry/profile.html>

Supporting information for this article is available on the WWW under <http://dx.doi.org/10.1002/ejic.201301288>

are various methods reported for the synthesis of ZnS, very little work has been performed on the synthesis of hybrid structures<sup>[23]</sup> of CSs and ZnS.

In the present work, we synthesized the hybrid material in two steps. In the first step, we prepared CSs by aerosol-assisted chemical vapor deposition (AACVD) of toluene at 1050 °C in the presence of nitrogen. Previously, the use of benzene/ferrocene-based aerosols was reported for the pyrolytic synthesis of aligned CNTs in the presence of Ar.<sup>[30]</sup> However, we did not employ any catalyst or template in the preparation of these nearly monodispersed spheres. In the second step, successive deposition of ZnS NPs on the surface of the CSs was achieved by solvothermal decomposition of a single-source precursor (SSP), that is, ZnCl<sub>2</sub>-(cinnamtszcz)<sub>2</sub> (cinnamtszcz = cinnamaldehyde thiosemicarbazone). The SSP molecule contains both metallic as well as nonmetallic parts, which are required for the synthesis of semiconducting NPs. Additionally, the use of a SSP minimizes toxicity and avoids contamination that occurs upon the separate introduction of two or more precursors. The solvothermal synthesis allows precise control over size, shape, and particle distribution and avoids the use of expensive chemicals. To the best of our knowledge, this is the first time that the use of a SSP has been reported for the preparation of a CSs–ZnS composite material by using the solvothermal method. We tested this material further in the photodegradation of methylene blue (MB) and eriochrome black-T (EBT) to emphasize the role of the CSs in the photocatalytic behavior of the ZnS NPs.

## Results and Discussion

### Crystalline CSs

Crystalline, monodispersed CSs were synthesized by AACVD of toluene at 1050 °C. The scanning electron microscopy (SEM) images recorded for the pristine product are shown in Figure 1 (a,b). Nearly isolated, uniformly spread spherical structures with an outer diameter of ca. 700 nm are observed. Energy-dispersive X-ray spectrometry (EDS) revealed the presence of 100% carbon (Figure S1, Supporting Information).

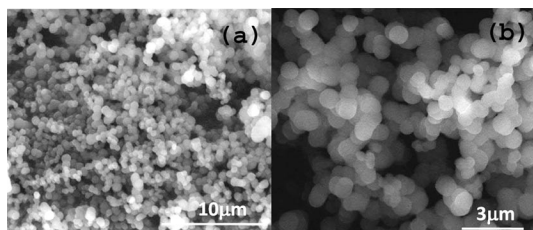


Figure 1. SEM images of pristine CSs prepared by AACVD of toluene: (a) low-magnification image and (b) high-magnification image.

The XRD pattern and Raman spectrum of the CSs are shown in Figure 2. A strong diffraction peak at 25.5° and a weaker peak at 43.3° in the XRD pattern of the CSs were assigned to characteristic diffractions, that is, (002) and

(101), reported for hexagonal graphitic carbon (JCPDS No. 75-1621). The broad nature of the peak indicates the presence of amorphous carbon in the sample.

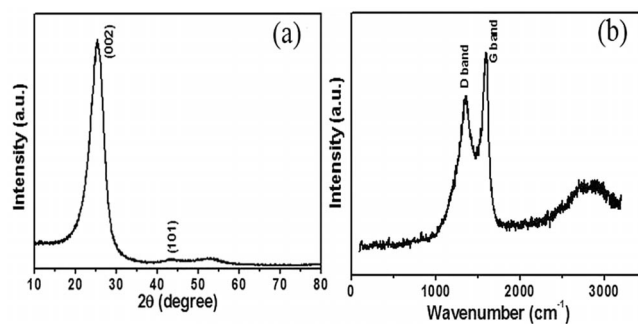


Figure 2. (a) XRD pattern and (b) Raman spectrum of pristine CSs prepared by AACVD of toluene.

In the Raman spectrum, two significant bands having peaks at about 1582 and 1354 cm<sup>-1</sup> and a single broad 2D band centered at 2830 cm<sup>-1</sup> are observed. The peak at 1582 cm<sup>-1</sup>, referred to as the G band, is associated with the E<sub>2g</sub> mode of hexagonal graphite and is related to the vibration of the sp<sup>2</sup>-hybridized carbon atoms in the graphite layer. A distinct band at 1354 cm<sup>-1</sup> (D band) is associated with the vibration of carbon atoms in the disordered graphite.<sup>[31]</sup> Its intensity increases with the number of graphitic layers present. The relative intensity ratio (I<sub>D</sub>/I<sub>G</sub>) signifies the degree of disorder in the graphitic structures. A higher ratio of I<sub>D</sub>/I<sub>G</sub> indicates a higher degree of disorder in the synthesized material. This ratio was found to be 0.76, which implies a relatively low proportion of defects in pristine CSs.<sup>[32]</sup>

A second feature in the Raman spectrum is a broad 2D band at ca. 2830 cm<sup>-1</sup>. This broadening could be due to the combination of the D and G bands, induced because of disorder.<sup>[33]</sup> Raman analysis suggests the presence of graphitic carbon in the product obtained by AACVD and is consistent with the result obtained from XRD. All these data reveal the formation of CSs in the sample obtained from the AACVD of toluene.

To ensure the purity and thermal stability of the CSs, thermogravimetric analysis (TGA) was performed under an inert atmosphere of N<sub>2</sub> (Figure 3, a) as well as in air (Figure 3, b). For TGA performed under an inert atmosphere, about 17% weight loss was observed, which was attributed to the loss of volatile solvent molecules, the oxidation of different functional groups associated with the CSs, which might be incorporated during the synthesis, and trace amounts of amorphous carbon present. In addition to this, the average particle size, surface area, and relative fractions of the edge sites in the spheres are known to contribute to the oxidation behavior of graphitic carbon materials.<sup>[34]</sup> These factors can further contribute to the decomposition behavior observed in the present case. No significant weight loss was observed up to 1000 °C, which suggests that the CSs are thermally stable. This could be assigned to the highly ordered graphitic structures. For TGA performed in air, as a result of the availability of sufficient oxygen, the

CSs were completely oxidized to give gaseous products and there was almost 100% weight loss up to 1000 °C. Similar observations were reported earlier.<sup>[16,17]</sup>

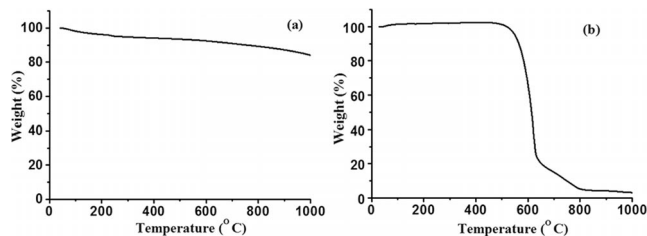


Figure 3. TGA profile of pristine CSs (a) under a N<sub>2</sub> atmosphere and (b) in air; heating rate: 10 °Cmin<sup>-1</sup>.

### CSs–ZnS Composite and ZnS NPs

The CSs–ZnS composite was prepared by heating the CSs with ZnCl<sub>2</sub>(cinnamtscz)<sub>2</sub> in ethylene glycol at reflux. ZnCl<sub>2</sub>(cinnamtscz)<sub>2</sub> acts as a SSP to give ZnS NPs. SSPs have many advantages over multiple source precursors. The main advantages of SSPs are their air stability, low toxicity, stoichiometric control of the synthesized materials, and low decomposition temperature. Similarly, the solvothermal method is beneficial owing to its simplicity and cleanliness. The experimental parameters that need to be controlled in a solvothermal route are very simple. This includes concentration of precursor, nature of solvent, and experimental time.

The utility of ZnCl<sub>2</sub>(cinnamtscz)<sub>2</sub> as a SSP for obtaining ZnS can be tested from TGA studies. TGA of this precursor under an inert atmosphere and in air gave ZnS and ZnO, respectively (Figure S2, Supporting Information). The weight loss (82.36%) observed in the TGA curve under an inert atmosphere matches that expected (82.18%) for ZnS (Figure S2a, Supporting Information). Whereas in air, the experimental weight loss (91.85%) tentatively matches the theoretical weight loss (85.12%) expected in the formation of ZnO (Figure S2b, Supporting Information).

The formation of the CSs–ZnS composite can be explained in two ways. First, the capping solvent molecules on the surface of ZnS can have interatomic bonding with the surface of the CSs, which results in the formation of the composite. Second, there may be direct deposition of ZnS NPs over the surface of the CSs. Such types of interactions are feasible as a result of the partial functionalization of the CSs during the synthesis. This is evident from the IR spectrum of the pristine CSs (Figure S3, Supporting Information). Similar kinds of interactions were proposed by Hu et al. They proposed that the functional groups present on the surface of the CSs can bind metal cations through coordination or electrostatic interaction.<sup>[35]</sup>

The XRD patterns of the ZnS NPs and the CSs–ZnS composite are shown in Figure 4 (a,b). The position of the diffraction peaks for CSs–ZnS and ZnS are in good agreement with the previous data and match well with the JCPDS file No. 79-2204.

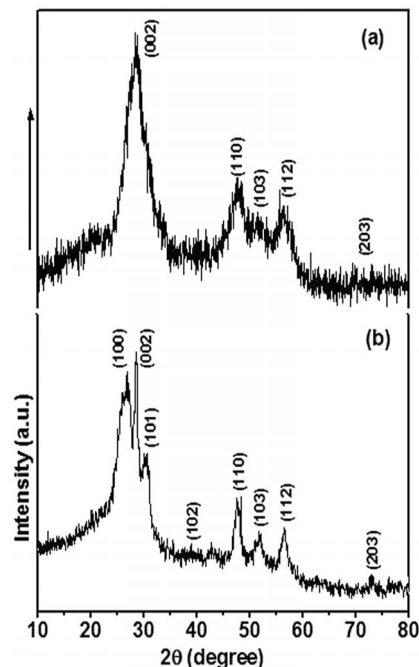


Figure 4. XRD patterns of the (a) ZnS NPs and (b) CSs–ZnS composite showing hexagonal phase of ZnS (JCPDS: 79-2204).

The peaks at 2θ values of 45, 55, and 70° correspond to the (001), (002), and (003) crystal planes of the hexagonal phase of ZnS. A peak at 25.5° corresponding to the characteristic (002) reflection of graphitic plane (JCPDS No. 75-1621) present in the CSs is merged with the (002) plane of ZnS. No other impurity or additional peaks are seen. Thus, there is exclusive formation of the CSs–ZnS composite.

The UV/Vis spectra recorded for the CSs, the CS–ZnS composite, and the ZnS NPs are shown in Figure S4 (Supporting Information). The absorption band at 279 nm observed for pristine CSs remains steady in the CSs–ZnS composite. This band could be assigned to the absorption of an aromatic π system in the graphitic structure.<sup>[36]</sup> The ZnS NPs show absorption at 339 nm (Figure S4c, Supporting Information), which is blueshifted to 329 nm in the CSs–ZnS composite (Figure S4b, Supporting Information). This could be assigned to a strong interaction between the CSs and ZnS, which might involve electron transfer from ZnS to CSs. The corresponding photoluminescence (PL) emission (excitation wavelength 320 nm) is shown in Figure 5 (a,b) for ZnS and ZnS in the CSs–ZnS composite. The PL spectrum shows a weak shoulder at 432 nm and a strong emission at 460 nm in the case of pure ZnS NPs. The former could be assigned to interstitial sulfur vacancies and lattice defects and the latter ZnS emission could result from Zn vacancies.<sup>[37]</sup> For the CSs–ZnS composite, the respective peaks are blueshifted to 406 and 426 nm. A drastic blueshift in the PL emission again suggests strong interaction between the ZnS NPs and the CSs; this is established through an electron-transfer process from the ZnS NPs to the CSs as previously observed for CNTs.<sup>[38]</sup>

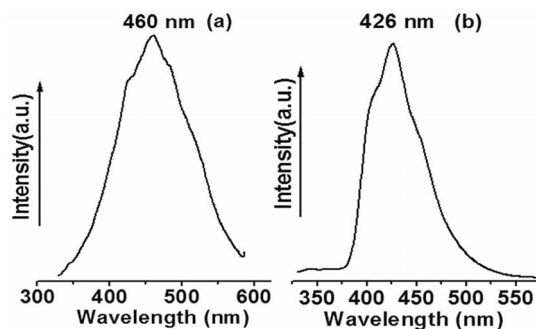


Figure 5. PL spectra of (a) ZnS NPs and (b) the CSs-ZnS composite.

Comparison of the Raman spectrum of pristine CSs with that of the CSs-ZnS composite shows that the characteristic bands of CSs are weakened as a result of ZnS coating (Figure S5, Supporting Information).

The SEM images of the ZnS NPs and CSs-ZnS composite synthesized by using the solvothermal method are shown in Figure 6 (a,b). The ZnS NPs formed are uniform and have a spherical morphology. They seem to be agglomerated at certain positions. Close inspection of Figure 6 (b) reveals a coating of ZnS NPs all over the surface of the CSs. Additionally, at certain points accretion of the CSs is seen, which is absent in the bare CSs (refer to Figure 1). This could be due to accretion of the CSs in ethylene glycol prior to its coating with the ZnS NPs. Such a type of accretion was previously reported by Kang et al.<sup>[39]</sup> upon treating CSs with acetone. According to that report, the spheres are made up of graphitic flakes and are believed to exhibit many dangling bonds at their surfaces. As a result, they become chemically active, which leads to accretion.

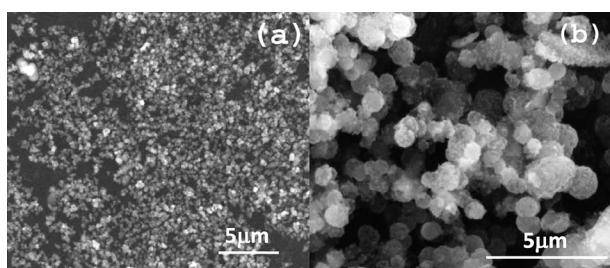


Figure 6. SEM images of (a) ZnS NPs and (b) the CSs-ZnS composite prepared by using the solvothermal method.

Figure 7 (a) reveals the TEM image recorded on pristine CSs. It shows nearly homogeneous, spherical, and transparent CSs with an average diameter of ca. 700 nm. The inset shows a single, isolated sphere overlapped with the other particles. Transparency is clearly visible in this overlapping. Figure 7 (b) shows ZnS NPs coated on CSs. The spheres look like faceted particles. The inset shows a single CS coated with ZnS NPs. The selected-area electron diffraction (SAED) pattern (Figure S6, Supporting Information) recorded on these samples clearly indicates (002) graphitic

reflections for CSs and planes for ZnS-coated CSs. Selective deposition of the ZnS NPs on the carbon spheres was observed and there is no unspecific precipitation in the solution. This may be attributed to interactions between the CSs and the ZnS NPs, as mentioned earlier. Moreover, the CSs provide surface for the growth of ZnS NPs. This is clearly seen in the TEM image of the composite.

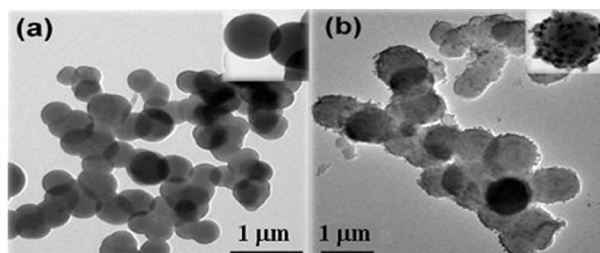
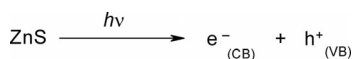


Figure 7. TEM images of (a) CSs and (b) the CSs-ZnS composite prepared by using the solvothermal method. Inset in (a) shows isolated CSs and the inset in (b) shows CSs coated with ZnS NPs.

### Photocatalytic Degradation Study

If a semiconductor material is exposed to the radiation of energy higher than its band gap energy, the photocatalytic process is initiated. In the case of ZnS NPs, the process can be represented as follows:



Electrons are scavenged by molecular oxygen to produce two intermediates, an oxygen radical and hydrogen peroxide. These immediately react amongst themselves to produce hydroxy radicals. These radicals are good oxidizing agents and are therefore responsible for the degradation of most of the dye molecules.<sup>[35]</sup>

The photodegradation efficiency of the CSs-ZnS composite was studied by recording the UV/Vis spectra for MB and EBT in the presence and absence of the catalyst. The results were compared with those obtained for ZnS NPs. Figure 8 (a,b) shows the photodegradation behavior of MB and EBT under UV irradiation performed in the presence of bare ZnS NPs and the CSs-ZnS composite. For comparison, the spectrum was also recorded for a solution without

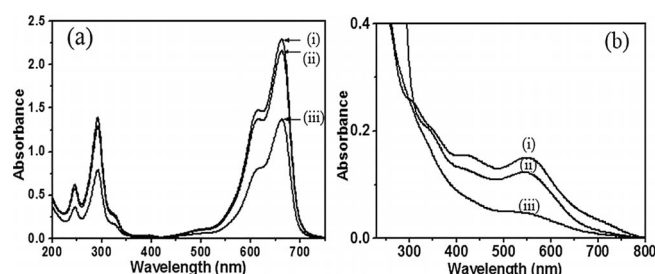


Figure 8. A comparative study of photodegradation of (a) MB and (b) EBT in the presence of (i) no catalyst (blank), (ii) ZnS NPs, and (iii) the CSs-ZnS composite.

any added catalyst. MB showed a greater decrease in the optical density in the presence of the CSs–ZnS composite than the sample with ZnS. Similarly, a decrease in optical density of the sample with ZnS was found to be greater relative to the optical density of the blank.

For EBT, an absorption band at 550 nm is observed, but the intensity of this band decreased substantially after UV irradiation in the presence of ZnS and CSs–ZnS. It seems that under identical experimental conditions, the rate of photodegradation is appreciably higher for the CSs–ZnS composite than for the bare ZnS NPs. This enhanced photocatalytic activity could be attributed to the presence of CSs in the composite. This can be further explained by using the study previously performed by Sun et al.<sup>[40]</sup> and Hu et al.<sup>[35]</sup> According to them, the surface of the CSs is hydrophilic and carries some functional groups on their surface; these groups have the capability to coordinate with metals. Moreover, there are some nanosized pores that are distributed on the surface of the spheres. This porosity not only provides the surface area but also promotes the penetration of some reactive species on the surface. Owing to this, a greater number of ZnS NPs is deposited on the surface of the CSs, which in turn facilitates the separation of the electrons and holes and avoids their recombination. This results in a higher concentration of the dye molecule near the ZnS NPs associated with the CSs, which ultimately leads to the effective degradation of the dye molecule.

## Conclusions

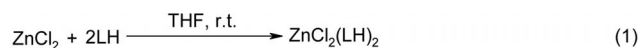
A simple solvothermal method with the use of a SSP was used for the synthesis of a CSs–ZnS composite. To the best of our knowledge, this is the first report on the synthesis of such a hybrid material by using a combination of AACVD and the solvothermal method and its successful use in the photodegradation of MB and EBT. The significant increase in photocatalytic efficiency was attributed to the large surface area and the porosity provided by the CSs for dye reduction.

## Experimental Section

**Synthesis of CSs by Using AACVD:** The setup used for the synthesis of the monodispersed CSs consisted of a single-zone furnace with an alumina tube (60 cm × 5 cm) and a thermocouple programmed with a temperature controller. A fused silica tube with a precleaned surface (70 cm × 3 cm) and having a standard B<sub>24</sub> joint was placed inside the single zone. A 250 mL round-bottomed flask containing toluene (40 mL) was attached to this tube with the help of a connector. The other end of the quartz tube was connected to a gas trap containing methanol to dissolve the byproducts formed during the reaction. The whole assembly was flushed with nitrogen gas, and nitrogen flow was continued throughout the experiment at a rate of ca. 190 mL min<sup>-1</sup>. The temperature of the furnace was raised to 1050 °C. Then, the mist of toluene generated by keeping the above flask on an ultrasonic humidifier was passed into this

preheated furnace. After the stipulated time, the humidifier was turned off to discontinue atomization, and the furnace was cooled in the presence of nitrogen. Then, the quartz tube was taken out, and the grayish product deposited on the wall of the tube was scratched and collected in a sample vial. The amount of precursor consumed was estimated by measuring the volume of the precursor solution before and after the experiment.

**Synthesis of the CSs–ZnS Composite and ZnS NPs by Using a SSP by the Solvothermal Method:** The single-source precursor, ZnCl<sub>2</sub>(cinnamtszcz)<sub>2</sub>, used in the present investigation was prepared by the method reported by our group.<sup>[41]</sup> Thus, cinnamaldehyde thiosemicarbazone dissolved in THF was added to a stoichiometric quantity of ZnCl<sub>2</sub> in THF, and the reaction mixture was stirred at room temperature for about 36 h. Then, the solvent was removed under vacuum, and the resulting yellow solid was repeatedly washed with cyclohexane to remove any impurities present. The product was dried under vacuum (m.p. 103 °C). The reaction scheme is shown in Equation (1).



For the synthesis of the CSs–ZnS composite and ZnS NPs, we slightly modified the procedure that was reported previously by our group for the synthesis of ZnS NPs.<sup>[41]</sup> In a typical experiment, a 250 mL, two-necked, round-bottomed flask was charged with CSs (60 mg). Ethylene glycol (20 mL) was then added, and the flask was sonicated for 30 min. Then, this flask was kept in a rotamantle, and the grayish black colored suspension obtained after sonication was stirred at reflux in the presence of nitrogen. In another separate 250 mL round-bottomed flask, ZnCl<sub>2</sub>(cinnamtszcz)<sub>2</sub> precursor (100 mg) was dissolved in ethylene glycol (20 mL). This solution was then injected by syringe into the above refluxing solution of CSs in ethylene glycol. The reaction was stirred for 1 h. After this time, the reaction mixture was cooled under an atmosphere of N<sub>2</sub>. The suspension obtained was centrifuged at 9000 rpm, washed thrice with dry methanol, and finally vacuum dried. The black-colored solid powder obtained was characterized by UV/Vis spectroscopy, PL spectroscopy, and Raman spectroscopy, in addition to XRD, SEM, and TEM techniques.

To synthesize the ZnS NPs, a 250 mL, two-necked, round-bottomed flask was charged with ethylene glycol (20 mL) and heated to reflux under an atmosphere of N<sub>2</sub>. In another 250 mL, single-necked round-bottomed flask, ZnCl<sub>2</sub>(cinnamtszcz)<sub>2</sub> (100 mg) was dissolved in ethylene glycol (20 mL). This solution was then injected by syringe into the round-bottomed flask containing refluxing ethylene glycol. After 1 h, the reaction mixture was cooled under an atmosphere of N<sub>2</sub>. The precipitate obtained was centrifuged at 5000 rpm, washed thrice with dry methanol, and finally vacuum dried. The white-colored solid powder obtained was characterized further with UV/Vis spectroscopy and PL spectroscopy, in addition to XRD, SEM, and TEM techniques.

**Material Characterization:** Powder XRD studies of the materials were performed with an XRD-7000, Shimadzu X-ray diffractometer by using Cu-K<sub>α</sub> radiation at a scan rate of 0.5° min<sup>-1</sup>. Raman spectra of the CSs and CSs–ZnS composite were recorded by using the 514 nm line from a diode pumped Nd<sup>3+</sup>:YAG laser (RENISHAW in via Raman Microscope, Laser 514 nm, Lens 100×). FTIR spectra were recorded with a Perkin–Elmer FTIR spectrophotometer. Analysis was performed by mixing the dried

samples with KBr followed by pressing it into a tablet. TGA of the CSs was performed with a Perkin–Elmer instrument, Pyris Diamond TG/DTA analyzer at a heating rate of 10 °Cmin<sup>-1</sup> under a nitrogen atmosphere as well as in air. SEM images were recorded with a FEI Quanta – 200 scanning electron microscope at an accelerating voltage of 20 kV. EDS was performed with a spectroscope attached to an SEM. TEM and SAED were performed with a TECNAI-G2 20 ultrawin FEI Netherland microscope at an accelerating voltage of 200 kV. Samples for the TEM images were prepared by dispersing the dried powder in methanol and placing several drops of the suspension on holey carbon films supported by copper grids. The PL spectra were recorded with a Perkin–Elmer LS 55 fluorescence spectrometer, whereas absorption spectra were recorded by using a UV-2450 PC Shimadzu UV/Vis spectrophotometer at room temperature. For both measurements, a weighed dried powder sample was dispersed in methanol and used to record the spectra.

**Comparative Study of CSs–ZnS and ZnS for Photodegradation of MB and EBT:** Photocatalytic activity studies of both the CSs–ZnS composite and ZnS NPs were performed. The photodegradation of MB and EBT in the presence of these materials was studied. Visible light from a 500 W Xe lamp with a 420 nm cutoff filter was used. MB and EBT of analytical reagent grade were used without any further purification. Initially, a stock solution ( $\delta = 200$  ppm) of each dye was prepared by dissolving its specific quantity in double-distilled water. Further concentrations were prepared by diluting the solution from the respective stock.

In a typical experiment, a 20 ppm solution of MB was prepared from the stock. An aliquot (100 mg) of each sample, ZnS and CSs–ZnS, was taken into two separate stoppered glass tubes. To this, the 20 ppm solution of MB (100 mL) was added, and the solution was sonicated for 30 min. These were then allowed to stir for 1 h to reach an adsorption–desorption equilibrium among the photocatalyst. In a separate glass tube, the 20 ppm solution of MB (100 mL) was taken without adding any catalyst for a point of reference. All the tubes were then irradiated under UV light for the stipulated time. Irradiation was stopped after 1 h, and all the solutions were centrifuged at 9000 rpm and filtered through Whatman filter paper no. 41. Their UV/Vis spectra were recorded to evaluate the change in the optical density after irradiation. A similar experiment was repeated for EBT under identical experimental conditions.

**Supporting Information** (see footnote on the first page of this article): EDS of the pristine CSs; TGA of ZnCl<sub>2</sub>(cinnamtsz)<sub>2</sub> under a N<sub>2</sub> atmosphere and in air; IR spectrum of the pristine CSs; UV/Vis spectra of the pristine CSs, the CSs–ZnS composite, and the ZnS NPs; Raman spectra of the pristine CSs and the CSs–ZnS composite; SAED patterns of the pristine CSs and the CSs–ZnS composite.

## Acknowledgments

K. M. S. wishes to acknowledge University Grants Commission (UGC), New Delhi for a Dr. D. S. Kothari Postdoctoral Fellowship. The authors wish to acknowledge Icon Analytical for providing the SEM facility for the research conducted.

[1] C. Xu, L. Cheng, P. Shen, Y. Liu, *Electrochem. Commun.* **2007**, *9*, 997–1001.

- [2] R. Cui, C. Liu, J. Shen, D. Gao, J. J. Zhu, H. Y. Chen, *Adv. Funct. Mater.* **2008**, *18*, 2197–2204.
- [3] Y. G. Wang, Y. Korai, I. Mochida, *Carbon* **1999**, *37*, 1049–1057.
- [4] R. Alcántara, F. J. Fernández Madrigal, P. Lavela, J. L. Tirado, J. M. Jiménez Mateos, C. G. de Salazar, R. Stoyanova, E. Zhecheva, *Carbon* **2000**, *38*, 1031–41.
- [5] F. Su, X. S. Zhao, Y. Wang, L. Wang, J. Y. Lee, *J. Mater. Chem.* **2006**, *16*, 4413–4419.
- [6] J. Lee, S. Yoon, T. Hyeon, S. M. Oh, K. B. Kim, *Chem. Commun.* **1999**, 2177–78.
- [7] R. Ryoo, S. H. Joo, S. Jun, *J. Phys. Chem. B* **1999**, *103*, 7743–7746.
- [8] J. S. Yu, S. B. Yoon, G. S. Chai, *Carbon* **2001**, *39*, 1442–1446.
- [9] A. Lu, A. Kiefer, W. Schmidt, F. Schuth, *Chem. Mater.* **2004**, *16*, 100–103.
- [10] X. Sun, Y. Li, *J. Colloid Interface Sci.* **2000**, *291*, 7–12.
- [11] Y. Xia, Z. Yang, R. Mokaya, *J. Phys. Chem. B* **2004**, *108*, 19293–19298.
- [12] N. A. Katcho, E. Urones-Garrote, D. Ávila-Brandé, A. Gómez-Herrero, S. Urbonaité, S. Csillag, E. Lomba, F. Agulló-Rueda, A. R. Landa-Cánovas, L. C. Otero-Díaz, *Chem. Mater.* **2007**, *19*, 2304–2309.
- [13] L. Ji, J. Ma, C. Zhao, W. Wei, L. Ji, X. Wang, M. Yang, Y. Lu, Z. Yang, *Chem. Commun.* **2006**, 1206–1208.
- [14] Y. Wang, D. Nepal, K. E. Geckeler, *J. Mater. Chem.* **2005**, *15*, 1049–1054.
- [15] X. Chen, K. Kierzek, Z. Jiang, H. Chen, T. Tang, M. Wojtoniszak, R. J. Kalenczuk, P. K. Chu, E. Borowiak-Palen, *J. Phys. Chem. C* **2011**, *115*, 17717–17724.
- [16] G. E. J. Poinern, S. Brundavanam, M. Shah, I. Laava, D. Fawcett, *Nanotechnol., Sci. Appl.* **2012**, *5*, 49–59.
- [17] Y. Z. Jin, C. Gao, W. K. Hsu, Y. Zhu, A. Huczko, M. Bystrzejewski, M. Roe, C. Y. Lee, S. Acquah, H. Kroto, D. R. M. Walton, *Carbon* **2005**, *43*, 1944–1953.
- [18] H. P. Cong, S. H. Yu, *Adv. Funct. Mater.* **2007**, *17*, 1814–1820.
- [19] H. Yu, J. Yu, S. Liu, S. Mann, *Chem. Mater.* **2007**, *19*, 4327–4334.
- [20] W. M. Zhang, J. S. Hu, Y. G. Guo, S. F. Zheng, L. S. Zhong, W. G. Song, L. G. Wan, *Adv. Mater.* **2008**, *20*, 1160–1165.
- [21] P. Wu, N. Du, H. Zhang, C. Zhai, D. Yang, *ACS Appl. Mater. Interfaces* **2011**, *3*, 1946–1952.
- [22] S. Tang, Y. Tang, S. Vongehr, X. Zhao, X. Meng, *Appl. Surf. Sci.* **2009**, *255*, 6011–6016.
- [23] S. V. Pol, V. G. Pol, A. Gedanken, *J. Phys. Chem. C* **2007**, *111*, 13309–13314.
- [24] L. Kong, X. Lu, X. Bian, W. Zhang, C. Wang, *Langmuir* **2010**, *26*, 5985–5990.
- [25] P. X. Hou, H. Orikasa, T. Yamazaki, K. Matsuoka, A. Tomita, N. Setoyama, Y. Fukushima, T. Kyotani, *Chem. Mater.* **2005**, *17*, 5187–5193.
- [26] T. Nakajima, M. Koh, M. Takashima, *Electrochim. Acta* **1998**, *43*, 883–891.
- [27] W. H. Zhang, J. L. Shi, H. R. Chen, Z. L. Hua, D. S. Yan, *Chem. Mater.* **2001**, *13*, 648–654.
- [28] R. N. Bhargava, D. Gallagher, X. Hong, A. Nurmikko, *Phys. Rev. Lett.* **1994**, *72*, 416–419.
- [29] Y. Ni, X. Cao, G. Hu, Z. Yang, X. Wei, Y. Chen, J. Xu, *Cryst. Growth Des.* **2007**, *7*, 280–285.
- [30] M. Mayne, N. Grobert, M. Terrones, R. Kamalakaran, M. Rühle, H. W. Kroto, D. R. M. Walton, *Chem. Phys. Lett.* **2001**, *338*, 101–107.
- [31] K. S. Subrahmanyam, S. R. C. Vivekchand, A. Govindaraj, C. N. R. Rao, *J. Mater. Chem.* **2008**, *18*, 1517–1523.
- [32] Y. Li, C. Zhou, X. Xie, G. Shi, L. Qu, *Carbon* **2010**, *48*, 4190–4196.
- [33] M. A. Pimenta, G. Dresselhaus, M. S. Dresselhaus, L. G. Cancado, A. Jorio, R. Saito, *Phys. Chem. Chem. Phys.* **2007**, *9*, 1276–1291.

- [34] W. Jiang, G. Nadeau, K. Zaghbi, K. Kinoshita, *Thermochim. Acta* **2000**, *351*, 85–93.
- [35] Y. Hu, Y. Liu, H. Qian, Z. Li, J. Chen, *Langmuir* **2010**, *26*, 18570–18575.
- [36] H. Li, X. He, Y. Liu, H. Huang, S. Lian, S. T. Lee, Z. Kang, *Carbon* **2011**, *49*, 605–609.
- [37] S. Wageh, Z. S. Ling, X. X. Rong, *J. Cryst. Growth* **2003**, *255*, 332–337.
- [38] J. Du, L. Fu, Z. Liu, B. Han, Z. Li, Y. Liu, Z. Sun, D. Zhu, *J. Phys. Chem. B* **2005**, *109*, 12772–12776.
- [39] Z. C. Kang, Z. L. Wang, *J. Phys. Chem.* **1996**, *100*, 5163–5165.
- [40] X. Sun, Y. Li, *Angew. Chem.* **2004**, *116*, 607–611; *Angew. Chem. Int. Ed.* **2004**, *43*, 597–601.
- [41] A. M. Palve, S. S. Garje, *J. Cryst. Growth* **2011**, *326*, 157–162.

Received: October 2, 2013

Published Online: December 9, 2013